Inorganic Chemistry

pubs.acs.org/IC

Article

Structural, Electronic, and Thermal Properties of $CdSnAs_2$

Wilarachchige D. C. B. Gunatilleke, Dean Hobbis, Hagen Poddig, Austin Tinkess, Matt Beekman, Hsin Wang, Kaya Wei, Ryan E. Baumbach, and George S. Nolas*

Cite This: *Inorg. Chem.* 2020, 59, 3079–3084

Read Online

ACCESS | Metrics & More | Article Recommendations

ABSTRACT: Structural, electrical, and thermal properties of $CdSnAs_2$, with analyses from temperature-dependent transport properties over a large temperature range, are reported. Phase-pure microcrystalline powders were synthesized that were subsequently densified to a high-density homogeneous polycrystalline specimen for this study. Temperature-dependent transport indicates *n*-type semiconducting behavior with a very high and nearly temperature independent mobility over the entire measured temperature range, attributed to the very small electron effective mass of this material. The Debye model was successfully applied to model the thermal conductivity and specific heat. This work contributes to the fundamental understanding of this material, providing further insight and allowing for investigations into altering this and related physical properties of these materials for technological applications.

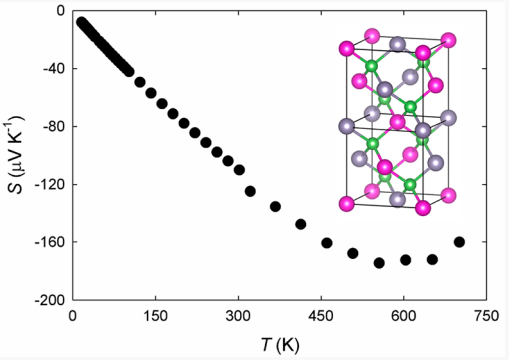

INTRODUCTION

Tetragonal chalcopyrites with a general formula of II−IV−V_2 continue to be of interest for a variety of applications, including optoelectronics and photovoltaics,[1−8] nonlinear optics,[9−12] topological insulators,[13] and spintronics.[14,15] Tetragonal ternary arsenides with lower-mass cations, i.e., II = Zn and IV = Si or Ge, have been the primary focus in the search for materials with specific properties of interest for these applications.[16−21] Moreover, these materials have been reported to possess low phonon group velocities and large Gruneisen parameters, which would indicate relatively low lattice thermal conductivities for this material system.[22] Most recently, the thermoelectric properties of antimony-based materials have also begun to be investigated.[23,24] Nevertheless, these materials have been investigated far less than chalcogenide compositions.

The crystal structure of II−IV−V_2 two-cation tetragonal ternary compositions can be considered a superstructure formed by the combination of the unit cells of two zinc-blende II−V and IV−V binaries thereby doubling the unit cell in the *c* direction resulting in a tetragonal unit cell. There are specific structural characteristics when comparing the binary cubic and ternary tetragonal structure types that reveal specific bonding and symmetry in these ternary compositions[25] and indicate similarities in their electronic structures. In both structure types, each cation shows a tetrahedral coordination by four anions; however, the two different cation types that are bonded to each of the anions cause the anions to shift to an equilibrium position creating a difference in bond lengths often reflected in the lattice parameter ratio $c/2a$ being <1.0.[26]

In this work, we report on the synthesis, structure, electrical, and thermal properties of *n*-type $CdSnAs_2$, a material that possesses a high electron mobility due to the very low electron effective mass and nonparabolic conduction band that is best described by Kane's model.[27] High-mobility materials are best for thermoelectrics as they permit optimization of the electronic properties, i.e., simultaneous optimization of the Seebeck coefficient and electrical conductivity, at lower doping levels than for low-mobility materials. This II−IV−V_2 composition may therefore be of particular interest for thermoelectric applications. Furthermore, our data extend to a wide temperature range for several of the properties reported herein, allowing for analyses of the intrinsic, low-temperature, physical properties as well as higher-temperature properties in the range of interest for thermoelectrics applications. Our fundamental investigation of $CdSnAs_2$ not only is of fundamental interest but may be of greatest interest in presenting the intrinsic properties of this material for further investigations aimed at doping, alloying, or composites targeting the desired properties for specific applications.

EXPERIMENTAL SECTION

Phase-pure $CdSnAs_2$ was synthesized by reaction of Cd chunks (99.99%, Alfa Aesar), Sn powder (99.99%, Alfa Aesar), and As

Received: November 21, 2019
Published: February 12, 2020

https://dx.doi.org/10.1021/acs.inorgchem.9b03424
Inorg. Chem. 2020, 59, 3079−3084

powder (99.9%, Alfa Aesar) with a 1:1:2 compositional ratio. The elements were sealed in an evacuated silica ampule and subjected to specific temperature treatment, modified from a previous report,[28] which resulted in a high-quality phase-pure microcrystalline product. The ampule was heated to 873 K at a rate of 20 K/h and held for 2 h. The temperature was then increased to 948 K at a rate of 20 K/h and held for 15 h. A multistep cooling process was employed where the temperature was initially decreased to 923 K at a rate of 20 K/h before being decreased to 823 K at a rate of 2 K/h. Finally, the specimen was cooled to 473 K at a rate of 10 K/h before the furnace was turned off. The resulting product was in the form of a polycrystalline ingot and was subsequently ground and sieved (325 mesh) prior to hot press densification. A custom-designed graphite die and molybdenum alloy punch assembly was used for hot pressing at 673 K and 150 MPa for 3 h under a continuous flow of ultra-high-purity N_2, resulting in a dense pellet of 98% theoretical density. The phase purity and structure were investigated from powder X-ray diffraction (XRD) data collected by a Bruker D8 Focus diffractometer in Bragg–Brentano geometry with Cu Kα radiation and a graphite monochromator. The stoichiometry and homogeneity were analyzed by Rietveld refinement using Jana2006.[29] Differential thermal analysis (DTA) and thermogravimetric analysis (TGA) were performed with a TA Instruments Q600 apparatus.

The densified specimen was cut into a 2 mm × 2 mm × 5 mm parallelepiped by a wire saw to determine the low-temperature (12–300 K) Seebeck coefficient, S, four-probe resistivity, ρ, and steady state thermal conductivity, κ, measurements on a custom-built radiation-shielded vacuum probe.[30,31] Electrical contacts were made by direct soldering onto nickel-plated surfaces, while Stycast epoxy was used for the thermal contacts. The maximum experimental uncertainties for S, ρ, and κ are 6%, 7%, and 8%, respectively. A second 2 mm × 1 mm × 10 mm parallelepiped was used for high-temperature (300–700 K) four-probe S and ρ measurements under −0.05 MPa static He in a ULVAC ZEM-3 system with the experimental uncertainty between 5% and 8% for the entire temperature range. A 0.6 mm thick disc was used for high-temperature (300–700 K) laser flash diffusivity measurements under flowing Ar in a NETZSCH LFA475 system with an experimental uncertainty of 5%. The relationship $\kappa = DdC_v$ was used to calculate κ, where D is the measured density, d is the measured thermal diffusivity, and the Dulong–Petit limit was used to estimate the specific heat, C_v, as these temperatures were well above the Debye temperature, as described below. The Hall coefficient was measured in the temperature range of 8–300 K using a custom system equipped with a He closed cycle cryostat and electromagnet in magnetic fields from −0.25 to 0.25 T. The Hall voltage showed a linear response to field at all temperatures, with an experimental uncertainty in the measured values of approximately 10%. The isobaric heat capacity, C_p, was measured from 1.8 to 250 K using a commercial Quantum Design physical property measurement system.

RESULTS AND DISCUSSION

Experimental, calculated, and difference diffraction patterns, produced by Rietveld refinement of the structure of $CdSnAs_2$, are shown in Figure 1, with results of the refinement listed in Tables 1 and 2. The structure was refined using the $I\bar{4}2d$ (No. 122) space group, and the ratio of the lattice parameters $c/2a$ gives a value of 0.98, reflecting a shift in the position of the anions due to the presence of two different cations compared to the ratio of 1.0 expected for the binary counterpart.[26,32] The refined x parameter for the As atoms at Wyckoff position 8d (x, $^1/_4$, $^1/_8$) is slightly shifted from the ideal chalcopyrite position of $^1/_4$[33] to 0.2422(1). Compositional stability analysis by DTA and TGA measurements, as shown in Figure 2, indicates that $CdSnAs_2$ is stable up to 873 K.

Figure 3 shows the temperature-dependent S values. The good agreement between the low- and high-temperature data, measured on separate specimens cut from the same pellet,

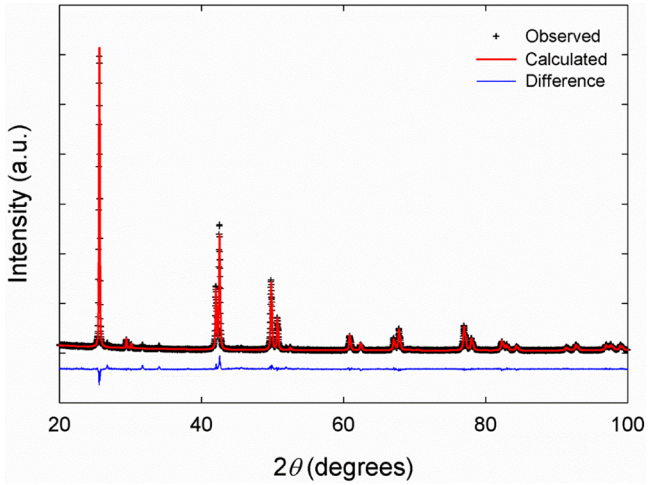

Figure 1. Powder XRD data for $CdSnAs_2$, including the profile fit and profile difference from Rietveld refinement.

Table 1. Rietveld Refinement Parameters

nominal composition	$CdSnAs_2$
refined composition	$CdSnAs_2$
space group	$I\bar{4}2d$ (No. 122)
$a = b$ (Å)	6.0988(6)
c (Å)	11.9257(2)
V (Å^3)	443.5(9)
radiation	graphite monochromator Cu Kα (1.54056 Å)
D_{calc} (g/cm^3)	5.70
2θ range (deg)	20–100
step width (deg)	0.02
wR_p, R_p	0.0323, 0.0271
reduced χ^2	1.9

Table 2. Atomic Coordinates and Displacement Parameters

atom	x	y	z	U_{iso} (Å^2)	occupancy
Cd	0	0	0	0.023(3)	1.0
Sn	0	0	0.5	0.013(3)	1.0
As	0.2422(1)	0.25	0.125	0.010(5)	1.0

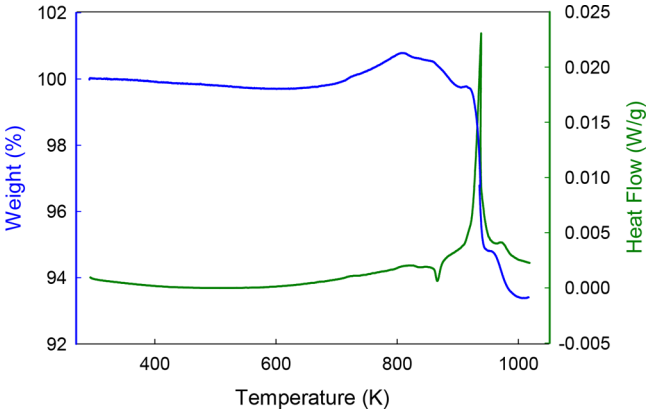

Figure 2. DTA (green) and TGA (blue) data for $CdSnAs_2$.

reflects the homogeneity of our polycrystalline specimen as well as the accuracy of the measurements. The S values are negative over the entire measured temperature range, indicating n-type conduction. Furthermore, the temperature dependence is typical of a semiconductor with S values that

https://dx.doi.org/10.1021/acs.inorgchem.9b03424
Inorg. Chem. 2020, 59, 3079–3084

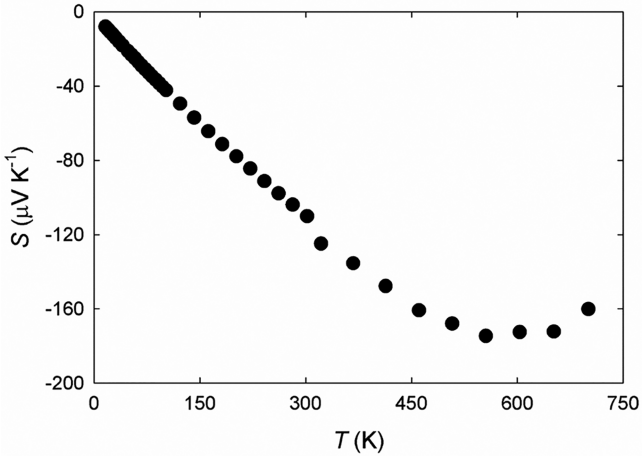

Figure 3. Temperature-dependent S data for $CdSnAs_2$.

increase with an increase in temperature until a maximum in S is reached at 550 K. From the data shown in Figure 3, the band gap, E_g, is estimated to be 0.20 eV employing the equation $S_{max} = E_g/2eT_{max}$, where S_{max} is the maximum value of S, e is the charge of an electron, and T_{max} is the temperature at which S_{max} occurs.[34] The temperature-dependent ρ values are shown in Figure 4, where $\ln(\rho)$ versus $1/T$ is plotted so that the solid

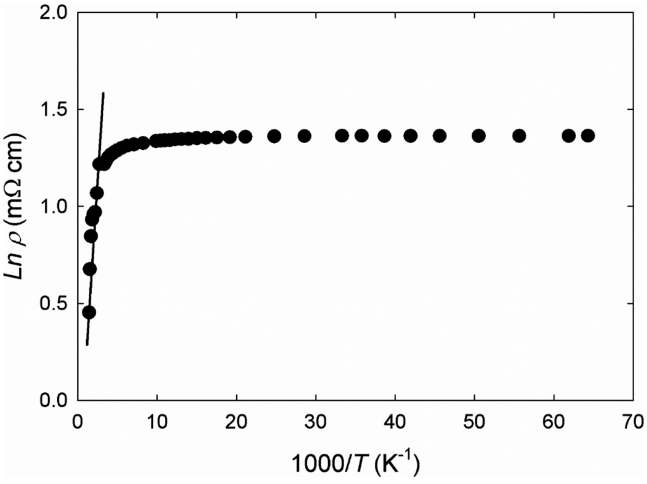

Figure 4. $\mathrm{Ln}(\rho)$ vs $1000/T$, where the solid line is a fit of the form $\rho = \rho_0 \exp(E_g/2k_BT)$, resulting in an E_g of 0.22 eV.

line fit to the highest-temperature data is of the form $\rho = \rho_0 \exp(E_g/2k_BT)$, where k_B is the Boltzmann constant and E_g = 0.22 eV from the fit. The values for E_g from our S and ρ data are in very good agreement with not only each other but also the previously reported value of 0.23 eV from infrared absorption data.[35]

The measured Hall coefficient, R_H, between 8 and 300 K is found to be relatively temperature independent at a value of -6.7 cm^3/C. The negative sign of R_H is in agreement with electrons as the majority charge carriers. The sign, magnitude, and temperature dependence of R_H suggest a low concentration of very shallow donors presumably from intrinsic compositional defects. Figure 5 shows the temperature-dependent Hall mobility, μ_H, deduced from Hall and resistivity measurements. The room-temperature μ_H is ~1600 cm^2 V^{-1} s^{-1} and is relatively temperature independent down to 8 K. This high value for μ_H for our polycrystalline specimen is

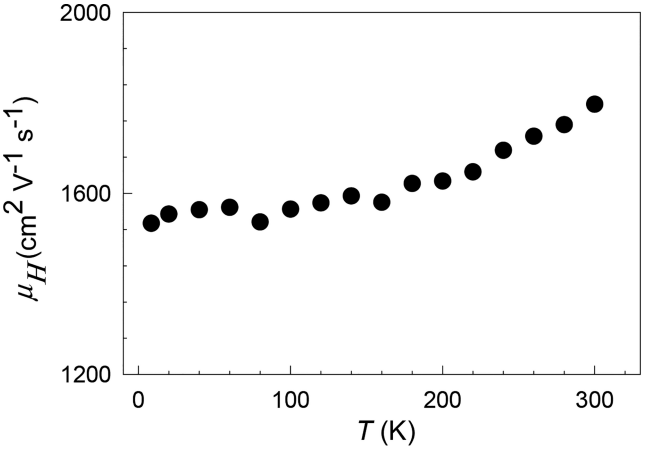

Figure 5. Temperature-dependent μ_H data for $CdSnAs_2$.

within a factor of 3 compared with that reported for single-crystal $CdSnAs_2$ and other high-mobility crystals[27,36] and can be attributed in part to the low effective mass for electrons in this material ($m^* \sim 0.04m_0$[37]). The high mobility is also another indication of the high quality and homogeneity of our polycrystalline specimen. The observation that the mobility is nearly temperature independent, and increases slightly at higher temperature, suggests that phonon scattering of the electrons is not the dominant scattering mechanism in the investigated temperature range. This may be attributed to the small electron effective mass in this material; for example, a small m^* tends to result in large and small scattering relaxation times in the cases of acoustic phonon (deformation potential) and ionized impurity scattering,[38] respectively. Thus, for small m^* values, the latter can dominate over the former even at relatively high temperatures.

Figure 6 shows C_p values for $CdSnAs_2$ as a function of temperature. The inset in the figure shows C_p/T versus T^2 data and a fit of the form $C_p/T = \gamma + \beta T^2$ for the low-temperature data, where γ is the Sommerfeld coefficient of the electronic contribution and β is the coefficient of the lattice contribution.[39] From this fit, we obtain $\gamma = -0.06$ mJ mol^{-1}

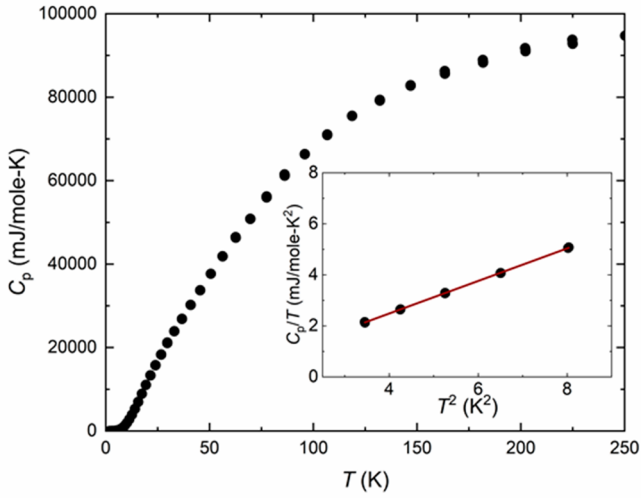

Figure 6. Temperature-dependent C_p data for $CdSnAs_2$ with the inset showing C_p/T vs T^2 at low temperatures, where the solid line is a fit of the form $C_p/T = \gamma + \beta T^2$.

https://dx.doi.org/10.1021/acs.inorgchem.9b03424
Inorg. Chem. 2020, 59, 3079−3084

K^{-2}, in effect a null value indicative of the negligible electronic contribution to C_p at these low temperatures, as expected for a material with a relatively low density of electrons and a very low m^*. Using the relation[39]

$$\theta_D = \left(\frac{12\pi^4 R n_a}{5\beta}\right)^{1/3} \quad (1)$$

where R is the molar gas constant, n_a is the number of atoms per formula unit, and β = 0.64 mJ mol^{-1} K^4 from our low-temperature fit (inset to Figure 6), we estimate the effective θ_D to be 228 K, in good agreement with the value reported by Hugon et al.[40]

Figure 7 shows the lattice contribution to the thermal conductivity, κ_L, estimated from κ using the Wiedemann–Franz relation $\kappa_e = L_0 T/\rho$, where $\kappa = \kappa_e + \kappa_L$ and L_0 is the Lorenz number. The solid line represents a theoretical fit to the data using the Debye–Callaway model:[41]

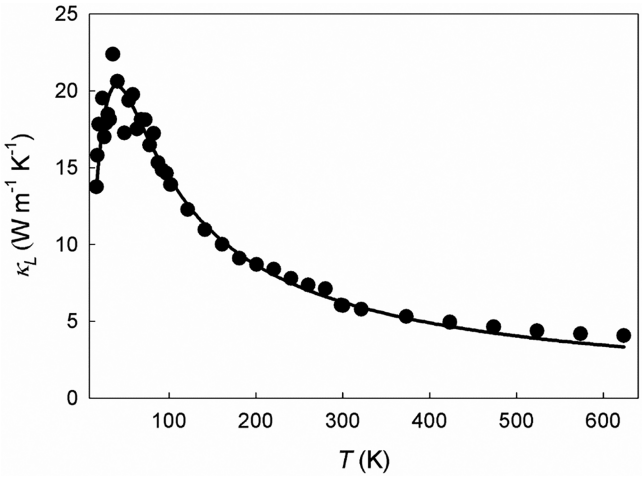

Figure 7. Temperature-dependent κ_L data for $CdSnAs_2$. The solid curve is a fit from the Debye–Callaway model.

$$\kappa_L = \frac{k_B}{2\pi^2 \upsilon}\left(\frac{k_B T}{\hbar}\right)^3 \int_0^{\theta_D/T} \frac{x^4 e^x}{\tau_C^{-1}(e^x - 1)^2}\, dx \quad (2)$$

where $x = \frac{\hbar\omega}{k_B T}$ is dimensionless, ω is the phonon frequency, $\hbar$ is the reduced Planck's constant, θ_D is the Debye temperature, and υ is the velocity of sound. The phonon scattering relaxation time, τ_C^{-1}, is given by[42−44]

$$\tau_C^{-1} = \frac{\nu}{L} + A\omega^4 + B\omega^2 T \exp\left(-\frac{\theta_D}{3T}\right) \quad (3)$$

where L is the grain size, ω_0 is the resonance frequency, and the coefficients A and B are fitting parameters related to the strength of the phonon scattering processes. The three terms in eq 3 represent grain boundary scattering, point defect scattering, and Umklapp scattering, respectively. As similarly observed in the electrical properties, the excellent agreement between the low- and high-temperature κ_L data (i.e., the data overlap and agree well at room temperature, although two separate pieces of different sizes and/or dimensions were measured on two different measurement systems) is another indication of the excellent homogeneity of our material and the accuracy of the measurements. Moreover, the Debye model fits the data very well throughout the entire measured temperature range.

The value for υ used in the fit was estimated from θ_D resulting in a υ of 2380 ms^{-1} [$\theta_D = \upsilon(h/k_B)(3n_a N_A d/4\pi M_w)^{1/3}$, where h is Planck's constant, N_A is Avogadro's constant, d is the density, and M_w is the molecular weight]. The following values were obtained from the fit: L = 6 μm, $A = 20.3 \times 10^{-43}$ s^3, and $B = 3.4 \times 10^{-18}$ K^{-1} s. The κ_L values show a T^3 temperature dependence in the low-temperature region, with a typical dielectric temperature dependence that peaks at 41 K. The A parameter is larger than that reported for $CoSb_3$ and $CuInSe_2$ single crystals,[45−48] as expected for our polycrystalline specimen; however, the B parameters of all three are relatively similar, implying similar low anharmonicity for these covalently bonded materials. The room-temperature κ_L of 6.0 W/mK is relatively high and consistent with the covalent nature of this material. We note the slight deviation in the fit relative to our experimental data at the highest temperatures suggests radiative heat loss at these temperatures.

CONCLUSION

The synthesis, structure, electrical, and thermal properties of polycrystalline n-type $CdSnAs_2$ are reported. Temperature-dependent ρ, S, and κ were measured over a large temperature range that allows for a thorough analysis of the physical properties from the obtained data and results. Rietveld refinement indicates a phase-pure specimen, and the transport properties indicate a high-quality polycrystalline specimen. The band gap, estimated from both ρ and S measurements, is approximately 0.2 eV, and specific heat data indicate θ_D to be 228 K. The κ_L values for this covalently bonded semiconductor are relatively high, in contrast to what has been reported previously,[22] with a typical dielectric temperature dependence. The electron mobility is very high, particularly for a polycrystalline specimen, with a relatively flat temperature dependence down to 1.8 K. This is of particular interest for thermoelectric applications as polycrystalline materials are typically used in these devices. Indeed, a relatively high thermoelectric figure of merit, ZT $(=S^2/\rho\kappa)$,[49] of 0.3 was obtained at 600 K for this unoptimized composition. This high ZT is due to the high power factor (S^2/ρ) for this material (see Figure 8), higher than that of recent quaternary chalcogenides and on par with those of chalcogenide chalcopyrite compounds

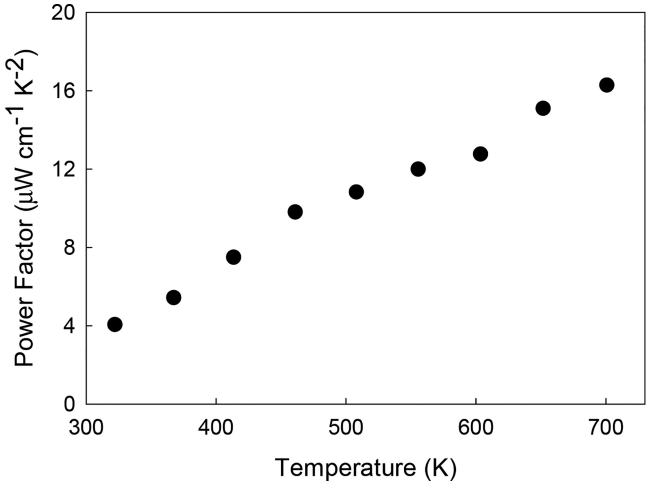

Figure 8. Temperature-dependent power factor data for $CdSnAs_2$.

https://dx.doi.org/10.1021/acs.inorgchem.9b03424
Inorg. Chem. 2020, 59, 3079−3084

such as $AgInSe_2$,[50−52] and illustrates their potential for thermoelectric applications. Alloying, doping, and nanoinclusions can be presumably employed to alter the electrical and thermal properties of these ternary arsenides and potentially improve the thermoelectric properties to enable further investigations for these applications.

AUTHOR INFORMATION

Corresponding Author

George S. Nolas − *Department of Physics, University of South Florida, Tampa, Florida 33620, United States;* orcid.org/0000-0001-8741-1678; Email: gnolas@usf.edu

Authors

Wilarachchige D. C. B. Gunatilleke − *Department of Physics, University of South Florida, Tampa, Florida 33620, United States*

Dean Hobbis − *Department of Physics, University of South Florida, Tampa, Florida 33620, United States*

Hagen Poddig − *Department of Physics, University of South Florida, Tampa, Florida 33620, United States; Faculty of Chemistry and Food Chemistry, Technische Universität Dresden, 01062 Dresden, Germany*

Austin Tinkess − *Department of Physics, California Polytechnic State University, San Luis Obispo, California 93407, United States*

Matt Beekman − *Department of Physics, California Polytechnic State University, San Luis Obispo, California 93407, United States*

Hsin Wang − *Materials Science and Technology Division, Oak Ridge National Laboratory, Oak Ridge, Tennessee 37831, United States*

Kaya Wei − *National High Magnetic Field Laboratory, Florida State University, Tallahassee, Florida 32310, United States*

Ryan E. Baumbach − *National High Magnetic Field Laboratory and Department of Physics, Florida State University, Tallahassee, Florida 32310, United States*

Complete contact information is available at: https://pubs.acs.org/10.1021/acs.inorgchem.9b03424

Notes

The authors declare no competing financial interest.

ACKNOWLEDGMENTS

This work was supported by National Science Foundation Grant DMR-1748188. H.P. acknowledges support by the ERASMUS+ ICM WORLDWIDE exchange program funded by the European Union. W.D.C.B.G. and D.H. acknowledge the II−VI Foundation Block-Gift Program. M.B. acknowledges funding from the William and Linda Frost Fund for instrumentation used in this work. K.W. acknowledges the support of the Jack E. Crow Postdoctoral Fellowship. A portion of this work was performed at the National High Magnetic Field Laboratory, which is supported by National Science Foundation Cooperative Agreement DMR-1644779 and the State of Florida. H.W. acknowledges support of the International Energy Agency (IEA) Advanced Materials for Transportation and the Department of Energy Lightweight and Propulsion Materials program under the Vehicle Technologies Office. Oak Ridge National Laboratory is managed by UT-Battelle LLC under Contract DE-AC05000OR22725.

REFERENCES

(1) Lincot, D.; Guillemoles, J. F.; Taunier, S.; Guimard, D.; Sicx-Kurdi, J.; Chaumont, A.; Roussel, O.; Ramdani, O.; Hubert, C.; Fauvarque, J. P.; Bodereau, N.; et al. Chalcopyrite thin film solar cells by electrodeposition. *Sol. Energy* **2004**, *77*, 725−737.

(2) Todorov, T.; Mitzi, D. B. Direct liquid coating of chalcopyrite light-absorbing layers for photovoltaic devices. *Eur. J. Inorg. Chem.* **2010**, *2010*, 17−28.

(3) Jäger-Waldau, A. In *Practical Handbook of Photovoltaics*; McEvoy, A., Markvart, T., Castañer, L., Eds.; Academic Press, 2012; Chapter IC-4, pp 373−395.

(4) Cao, Q.; Gunawan, O.; Copel, M.; Reuter, K. B.; Chey, S. J.; Deline, V. R.; Mitzi, D. B. Defects in Cu (In, Ga) Se_2 chalcopyrite semiconductors: A comparative study of material properties, defect states, and photovoltaic performance. *Adv. Energy. Mater.* **2011**, *1*, 845−853.

(5) Rockett, A. A. Current status and opportunities in chalcopyrite solar cells. *Curr. Opin. Solid State Mater. Sci.* **2010**, *14*, 143−148.

(6) Fiechter, S.; Tomm, Y.; Kanis, M.; Scheer, R.; Kautek, W. On the homogeneity region, growth modes and optoelectronic properties of chalcopyrite-type $CuInS_2$. *Phys. Status Solidi B* **2008**, *245*, 1761−1771.

(7) Fuertes Marron, D.; Cánovas, E.; Levy, M. Y.; Marti, A.; Luque, A.; Afshar, M.; Albert, J.; Lehmann, S.; Abou-Ras, D.; Sadewasser, S.; Barreau, N. Optoelectronic evaluation of the nanostructuring approach to chalcopyrite-based intermediate band materials. *Sol. Energy Mater. Sol. Cells* **2010**, *94*, 1912−1918.

(8) Kerroum, D.; Bouafia, H.; Sahli, B.; Hiadsi, S.; Abidri, B.; Bouaza, A.; Timaoui, M. A. Pressure effect on mechanical stability and optoelectronic behavior of zinc-silicon diarsenide $ZnSiAs_2$-chalcopyrite: DFT investigation. *Optik* **2017**, *139*, 315−327.

(9) Ohmer, M. C.; Pandey, R. Emergence of chalcopyrites as nonlinear optical materials. *MRS Bull.* **1998**, *23*, 16−22.

(10) Kildal, H.; Mikkelsen, J. C. The nonlinear optical coefficient, phasematching, and optical damage in the chalcopyrite $AgGaSe_2$. *Opt. Commun.* **1973**, *9*, 315−318.

(11) Abrahams, S. C.; Bernstein, J. L. Piezoelectric nonlinear optic $CuGaS_2$ and $CuInS_2$ crystal structure: Sublattice distortion in $A^IB^{III}C_2^{VI}$ and $A^{II}B^{IV}C_2^{V}$ type chalcopyrites. *J. Chem. Phys.* **1973**, *59*, 5415−5422.

(12) Boyd, G.; Buehler, E.; Storz, F.; Wernick, J. Linear and nonlinear optical properties of ternary $A^{II}B^{IV}C_2^{V}$ chalcopyrite semiconductors. *IEEE J. Quantum Electron.* **1972**, *8*, 419−426.

(13) Feng, W.; Xiao, D.; Ding, J.; Yao, Y. Three-Dimensional Topological Insulators in I−III−VI_2 and II−IV−V_2 Chalcopyrite Semiconductors. *Phys. Rev. Lett.* **2011**, *106*, 016402.

(14) Zhao, Y. J.; Zunger, A. Site preference for Mn substitution in spintronic $CuM^{III}X_2^{VI}$ chalcopyrite semiconductors. *Phys. Rev. B: Condens. Matter Mater. Phys.* **2004**, *69*, 075208.

(15) Koroleva, L. I.; Zashchirinskii, D. M.; Khapaeva, T. M.; Marenkin, S. F.; Fedorchenko, I. V.; Szymczak, R.; Krzumanska, B.; Dobrovol'skiĭ, V.; Kilanskii, L. Manganese-doped ZnSiAs 2 chalcopyrite: A new advanced material for spintronics. *Phys. Solid State* **2009**, *51*, 303−308.

(16) Shay, J. L.; Wernick, J. H. *Ternary chalcopyrite semiconductors: Growth, electronic properties and applications*; Pergamon Press: Oxford, U.K., 1975.

(17) Medvedkin, G. A.; Ishibashi, T.; Nishi, T.; Hayata, K.; Hasegawa, Y.; Sato, K. Room temperature ferromagnetism in novel diluted magnetic semiconductor $Cd_{1-x}Mn_xGeP_2$. *Jpn. J. Appl. Phys.* **2000**, *39*, L949.

(18) Cho, S.; Choi, S.; Cha, G. B.; Hong, S. C.; Kim, Y.; Zhao, Y. J.; Freeman, A. J.; Ketterson, J. B.; Kim, B. J.; Kim, Y. C.; Choi, B. C. Room-temperature ferromagnetism in $(Zn_{1-x}Mn_x)GeP_2$ semiconductors. *Phys. Rev. Lett.* **2002**, *88*, 257203.

(19) Erwin, S. C.; Žutić, I. Tailoring ferromagnetic chalcopyrites. *Nat. Mater.* **2004**, *3*, 410.

(20) Feigelson, R. S.; Route, R. K. Recent developments in the growth of chalcopyrite crystals for nonlinear infrared applications. *Opt. Eng.* **1987**, *26*, 262113.

(21) Sandroni, M.; Wegner, K. D.; Aldakov, D.; Reiss, P. Prospects of Chalcopyrite-Type Nanocrystals for Energy Applications. *ACS Energy Lett.* **2017**, *2*, 1076−1088.
(22) Mukherjee, M.; Yumnam, G.; Singh, A. K. High Thermoelectric Figure of Merit via Tunable Valley Convergence Coupled Low Thermal Conductivity in $A^{II}B^{IV}C_2^{V}$ Chalcopyrites. *J. Phys. Chem. C* **2018**, *122*, 29150−29157.
(23) Nomura, A.; Choi, S.; Ishimaru, M.; Kosuga, A.; Chasapis, T.; Ohno, S.; Snyder, G. J.; Ohishi, Y.; Muta, H.; Yamanaka, S.; Kurosaki, K. Chalcopyrite $ZnSnSb_2$: A Promising Thermoelectric Material. *ACS Appl. Mater. Interfaces* **2018**, *10*, 43682−43690.
(24) Liu, H.; Zhao, B.; Yu, Y.; He, Z.; Xiao, J.; Huang, W.; Zhu, S.; Chen, B.; Xie, L. Theoretical investigations on elastic, thermal and lattice dynamic properties of chalcopyrite $ZnSnX_2$ (X = P, As, Sb) under pressure and temperature: The first-principles calculation. *Int. J. Mod. Phys. B* **2018**, *32*, 1850329.
(25) Verma, A. S.; Bhardwaj, S. R. Inherent properties of complex structured solids. *Phys. Scr.* **2009**, *79*, 015302.
(26) Jaffe, J. E.; Zunger, A. Theory of the band-gap anomaly in ABC_2 chalcopyrite semiconductors. *Phys. Rev. B: Condens. Matter Mater. Phys.* **1984**, *29*, 1882.
(27) Hugon, P. L. Etude experimentale de la structure de bande du compose CdSnAs2. *J. Phys. Chem. Solids* **1966**, *27*, 1205−1218.
(28) Voevodin, V. G.; Bereznaja, S. A.; Voevodina, O. V.; Korotchenko, Z. V.; Fernelius, N. C.; Ohmer, M. C.; Goldstein, J. T. Doping of ternary compounds $CdGeAs_2$ and $CdSnAs_2$ by impurities of I, II and III groups. *J. Phys. Chem. Solids* **2003**, *64*, 1755−1760.
(29) Petříček, V.; Dušek, M.; Palatinus, L. Crystallographic Computing System JANA2006: General features. *Z. Kristallogr. - Cryst. Mater.* **2014**, *229*, 345−352.
(30) Martin, J.; Erickson, S.; Nolas, G. S.; Alboni, P.; Tritt, T. M.; Yang, J. Structural and transport properties of $Ba_8Ga_{16}Si_xGe_{30-x}$ clathrates. *J. Appl. Phys.* **2006**, *99*, 044903.
(31) Martin, J.; Nolas, G. S. Apparatus for the measurement of electrical resistivity, Seebeck coefficient, and thermal conductivity of thermoelectric materials between 300 and 12 K. *Rev. Sci. Instrum.* **2016**, *87*, 015105.
(32) Gasson, D.B.; Holmes, P.J.; Jennings, I.C.; Marathe, B.R.; Parrott, J.E. The Properties of $ZnSnAs_2$ and $CdSnAs_2$. *J. Phys. Chem. Solids* **1962**, *23*, 1291−1302.
(33) Knight, K. S. The crystal structures of $CuInSe_2$ and $CuInTe_2$. *Mater. Res. Bull.* **1992**, *27*, 161−167.
(34) Goldsmid, H. J.; Sharp, J. W. Estimation of the thermal band gap of a semiconductor from Seebeck measurements. *J. Electron. Mater.* **1999**, *28*, 869−872.
(35) Strauss, A. J.; Rosenberg, A. J. Preparation and properties of CdSnAs2. *J. Phys. Chem. Solids* **1961**, *17*, 278−283.
(36) Prince, M. B. Drift mobilities in semiconductors. *Phys. Rev.* **1953**, *92*, 681−687.
(37) Nakashima, Y.; Hamaguchi, C. Shubnikov-de Haas Oscillations in $CdSnAs_2$ Observed by Magnetic Field-Modulation Technique. *J. Phys. Soc. Jpn.* **1987**, *56*, 3248−3252.
(38) Li, S. S. *Semiconductor Physical Electronics*; Springer Science +Business Media: New York, 2006.
(39) Kittel, C. *Introduction to Solid State Physics*; John Wiley & Sons: New York, 1976.
(40) Hugon, P. L.; Veyssie, J. J. Proprietés thermiques des composés ternaires CdSnAs2 et ZnSnAs2. *Phys. Status Solidi B* **1965**, *8*, 561−568.
(41) Callaway, J. Model for lattice thermal conductivity at low temperatures. *Phys. Rev.* **1959**, *113*, 1046.
(42) Leibfried, G.; Schloemann, E. Thermal conductivity of dielectric solids by a variational technique. *Nachr. Akad. Wiss. Goettingen II* **1954**, *71*, 1366−1370.
(43) Slack, G. A.; Galginaitis, S. Thermal conductivity and phonon scattering by magnetic impurities in CdTe. *Phys. Rev.* **1964**, *133*, A253.
(44) Klemens, P. G. The scattering of low-frequency lattice waves by static imperfections. *Proc. Phys. Soc., London, Sect. A* **1955**, *A68*, 1113.
(45) Nolas, G. S.; Fowler, G.; Yang, J. Assessing the role of filler atoms on the thermal conductivity of filled skutterudites. *J. Appl. Phys.* **2006**, *100*, 043705.
(46) Lamberton, G. A., Jr; Bhattacharya, S.; Littleton IV, R. T.; Kaeser, M. A.; Tedstrom, R. H.; Tritt, T. M.; Yang, J.; Nolas, G. S. High figure of merit in Eu-filled $CoSb_3$-based skutterudites. *Appl. Phys. Lett.* **2002**, *80*, 598−600.
(47) Wasim, S. M.; Noguera, A. Transport properties of n-type $CuInSe_2$. *Phys. Status Solidi A* **1984**, *82*, 553−559.
(48) Nolas, G. S.; Yang, J.; Ertenberg, R. W. Transport properties of $CoGe_{1.5}Se_{1.5}$. *Phys. Rev. B: Condens. Matter Mater. Phys.* **2003**, *68*, 193206.
(49) Nolas, G. S.; Sharp, J.; Goldsmid, J. *Thermoelectrics: basic principles and new materials developments*; Springer-Verlag: Berlin, 2001.
(50) Wei, K.; Beauchemin, L.; Wang, H.; Porter, W. D.; Martin, J.; Nolas, G. S. Enhanced thermoelectric properties of $Cu_2ZnSnSe_4$ with Ga-doping. *J. Alloys Compd.* **2015**, *650*, 844−847.
(51) Dong, Y.; Wojtas, L.; Martin, J.; Nolas, G. S. Synthesis, crystal structure, and transport properties of quaternary tetrahedral chalcogenides. *J. Mater. Chem. C* **2015**, *3*, 10436−10441.
(52) Ying, P. Z.; Zhou, H.; Gao, Y. L.; Li, Y. Y.; Li, Y. P.; Lian, X. L.; Cui, J. L. Thermoelectric Properties of a Wide−Gap Chalcopyrite Compound $AgInSe_2$. *Key Eng. Mater.* **2012**, *519*, 188−192.

https://dx.doi.org/10.1021/acs.inorgchem.9b03424
Inorg. Chem. 2020, 59, 3079−3084